applied sciences

MDPI

Article

Numerical Modelling Assessment of the Impact of Hydrogen on the Energy and Environmental Performance of a Car Using Dual Fuel (Gasoline–Hydrogen)

Saugirdas Pukalskas *, Tadas Vipartas, Alfredas Rimkus, Donatas Kriaučiūnas, Justas Žaglinskis, Saulius Stravinskas, Andrius Ušinskas, Romualdas Juknelevičius, Gabrielius Mejeras, Vidas Žuraulis, Vilius Mejeras and Aleksas Narkevičius

Department of Automobile Engineering, Faculty of Transport Engineering, Vilnius Gediminas Technical University, Plytinės Str. 25, 10105 Vilnius, Lithuania; tadas.vipartas@vilniustech.lt (T.V.); alfredas.rimkus@vilniustech.lt (A.R.); donatas.kriauciunas@vilniustech.lt (D.K.); justas.zaglinskis@vilniustech.lt (J.Ž.); saulius.stravinskas@vilniustech.lt (S.S.); andrius.usinskas@vilniustech.lt (A.U.); romualdas.juknelevicius@vilniustech.lt (R.J.); gabrielius.mejeras@vilniustech.lt (G.M.); vidas.zuraulis@vilniustech.lt (V.Ž.); vilius.mejeras@vilniustech.lt (V.M.); aleksas.narkevicius@vilniustech.lt (A.N.)

* Correspondence: saugirdas.pukalskas@vilniustech.lt; Tel.: +370-655-29-573

Abstract: The utilization of "green" hydrogen in transportation areas gives rise to production- and supply infrastructure-related challenges; therefore, its wider application in automotive transport would lead to higher demand with cost reduction and a faster expansion of the hydrogen refuelling network. This study presents energy and environmental performance indicators analyses of a Nissan Qashqai J10 engine during the Worldwide Harmonised Light Vehicles Test Cycle (WLTC), replacing conventional fossil gasoline with dual-fuel (D-F) gasoline and hydrogen. Numerical modelling was conducted using AVL Cruise™ (Version R2022.2) software, utilizing the torque, fuel consumption, and environmental performance data of the HR16DE engine obtained through experimental testing across a wide range of loads and speeds on an engine test bench. The experimental investigation was carried out in two stages: using pure gasoline (G100); injecting a hydrogen additive into the intake air, constituting 5% of the gasoline mass (G95H5). Following similar stages, numerical modelling was conducted using the vehicle's technical specifications to calculate engine load and speed throughout the WLTC range. Instant fuel consumption and pollutant emissions (CO, CH, NO_x) were determined for various driving modes using experimental data maps. CO_2 emissions were calculated considering fuel composition and consumption. By integrating the instant values, the total and specific fuel consumption and emissions were calculated. As a result, this study identified the effect of a 5% hydrogen additive in improving engine energy efficiency, reducing incomplete combustion products and lowering greenhouse gas (CO_2) emissions under various driving modes. Finally, the results were compared with the requirements of EU standards.

Keywords: spark ignition engine; hydrogen; dual fuel; WLTC; AVL Cruise™ specific emissions

check for updates

Academic Editor: Nikolaos Koukouzas

Received: 21 December 2024
Revised: 24 January 2025
Accepted: 11 February 2025
Published: 13 February 2025

Citation: Pukalskas, S.; Vipartas, T.; Rimkus, A.; Kriaučiūnas, D.; Žaglinskis, J.; Stravinskas, S.; Ušinskas, A.; Juknelevičius, R.; Mejeras, G.; Žuraulis, V.; et al. Numerical Modelling Assessment of the Impact of Hydrogen on the Energy and Environmental Performance of a Car Using Dual Fuel (Gasoline–Hydrogen). *Appl. Sci.* **2025**, *15*, 1939. https://doi.org/10.3390/app15041939

Copyright: © 2025 by the authors. Licensee MDPI, Basel, Switzerland. This article is an open access article distributed under the terms and conditions of the Creative Commons Attribution (CC BY) license (https://creativecommons.org/licenses/by/4.0/).

1. Introduction

Greenhouse gas (GHGs: carbon dioxide (CO_2), nitrous oxide (N_2O), methane—CH_4, F-gasses, and water vapour (H_2O)) emissions increase across various sectors from three different base years—1990, 2005, and 2021—to 2022 as analyzed in the JRC (Joint Research

Centre—European Commission) science for policy report on GHG emissions of all world countries [1]. The power industry has seen a significant rise in emissions, with a 92% increase from 1990 and a 34% increase from 2005, alongside a modest 1% increase from 2021 to 2022. Similarly, the industrial combustion and processes sector experienced the largest surge, with a 95% increase from 1990 and a 43% increase from 2005. In the buildings sector, emissions had a slight increase of 3% from 2005. Agriculture emissions have steadily increased by 21% from 1990, 15% from 2005, and 1% from 2021 to 2022. The transport sector shows notable emission increases across all periods, with a 72% rise from 1990, a 22% increase from 2005, and a significant 5% rise from 2021 to 2022. The fuel exploitation sector also recorded substantial increases, with a 56% rise from 1990, a 22% increase from 2005, and a 3% rise from 2021.

Mathematical prediction models show that GHG emissions from the transport sector will tend to increase for most European countries for the next several years [2], while China's case shows a rise for both energy consumption and transport CO_2 emissions by 2050 [3]. Modern prediction models are mostly based on neural networks, metaheuristics, prediction factor selection, or hybrid technology, and some regions like the USA show inconsistent results for future emissions [4,5]. In contrast, low-income countries with fast GDP (gross domestic product) growth are facing a GHG emissions increase, and a decrease in energy intensity is one of this problem's solution [6].

Most nations globally are developing strategies to address climate change. The European Union (EU) is particularly proactive, with ambitious goals outlined in the European Green Deal and European Climate Law [7,8]. The EU aims to cut its net domestic GHG emissions by a minimum of 55% by 2030 compared to 1990 levels and achieve climate neutrality (net-zero GHG emissions) by 2050 [1].

Due to the reliance on fossil fuels, the transport sector is a significant contributor to GHG emissions, while the electric vehicle's part is still increasing [9]. Domestic transportation in EU 27 (27 member states of the European Union) follows closely, contributing 23.1%, which reflects the substantial impact of vehicles and transport systems on the environment [10]. Here, emissions initially increased significantly from approximately 672 $MtCO_2e$ (million metric tons of carbon dioxide equivalent) in 1990 to a peak of around 863 $MtCO_2e$ in 2007. This represents a 28.4% increase over 17 years, driven by growing vehicle usage and economic activity. After 2007, emissions from domestic transportation began to decline; however, by 2022, emissions increased up to ~803 $MtCO_2e$, reflecting a 3.8% reduction since 2014. Overall, from 1990 to 2022, there was a ~19.5% increase in emissions, despite the recent declines.

Hydrogen has emerged as a promising solution for reducing GHG emissions due to its potential for zero carbon emissions [11–19]. When burned, hydrogen produces only water as a by-product, thereby eliminating carbon dioxide emissions entirely [20–22]. Hydrogen's wide flammability limits and high flame propagation rates enable stable combustion, even with lean mixtures, which can significantly improve engine efficiency and reduce nitrogen oxide (NO_x) emissions [23]. Moreover, hydrogen has a higher energy content per unit mass compared to petrol, which can result in higher thermal efficiency for engines designed to utilize hydrogen effectively. Additionally, hydrogen's capability to produce power without emitting carbon compounds positions it as a superior alternative in the quest for cleaner automotive technologies; however, it depends on the type of hydrogen production, as so-called black, brown, grey, and blue hydrogen is indicated [24]. When used in spark ignition engines, hydrogen combustion produces no carbon monoxide (CO), CO_2, hydrocarbons (HC), or particulate matter (PM) emissions, making it an exceptionally clean fuel choice [25,26].

Hydrogen's high burning velocity and broad flammability range, in contrast to traditional fossil fuels, elevate the risk of flashbacks, pre-ignition, and accidental explosions [27–29]. Moreover, the combustion of pure hydrogen produces a high combustion temperature, leading to the formation of nitrogen oxides [30–32]. Using hydrogen as fuel at excess air ratios higher than 1.3 reduces NO_x emissions by up to six times compared to emissions at a stoichiometric mixture. Lean air–hydrogen mixtures combust at lower temperatures, which are not enough to support NO_x formation [33,34]. Adjusting spark timing can also help reduce NO_x emissions. At an excess air ratio of 1.4, retarding the spark timing by just 4 CAD (crank angle degrees) results in a 17% reduction in NO_x emissions. For instance, at an excess air ratio of 1.6, retarding the spark timing leads to a 70% reduction in NO_x emissions [35]. Selecting the specific mixture formation method like 'spark-plug mildly stratified charge', NOx emissions are limited to less than 10 ppm [36].

Due to its low energy density under standard temperature and pressure, hydrogen requires specialized storage solutions. For instance, a fuel cell vehicle requires approximately 5–6 kg of hydrogen, compressed to 700 bar, to achieve a driving range of 500 km [37]. Combusting hydrogen in an internal combustion engine (ICE) requires an even greater amount of hydrogen to be stored on board the vehicle. According to modelling results from Chalmers University of Technology, hydrogen fuel cell vehicles demonstrate nearly twice the efficiency of ICEs, with a lower fuel consumption of 1.05 kg-H_2 per 100 km under the Worldwide Harmonised Light Vehicles Test Procedure driving cycle (WLTC), compared to approximately 1.79 kg-H_2 per 100 km for hydrogen combustion vehicles [38]. Replacing petrol with hydrogen to achieve a driving range of at least 500 km presents significant challenges, primarily due to the increased amount of hydrogen that needs to be stored in the vehicle. Also, hydrogen is highly flammable, and special composite H_2 fuel tanks must be used for hydrogen storage. For fuelling systems, stainless steel lines are required, along with a special pressure reducer equipped with a flame arrestor. A hydrogen leak detection system should also be installed, incorporating hydrogen sensors that provide warnings and can automatically shut off the tank's main stop valves in the event of a leak. In case of a fire, a pressure relief system should vent hydrogen away from the vehicle and passengers to minimize the risk of explosions. Additionally, automatic shut-off valves should be installed to automatically close solenoid valves on the hydrogen tanks during a crash, isolating the fuel supply. Even with the installation of safety systems, dual-fuel technology remains a potential alternative for reducing greenhouse gas emissions and fossil fuel consumption.

One potential solution to the storage challenge is implementing a dual-fuel system. In this approach, hydrogen can be used as an additive or substitute for a small portion (up to 15% by mass) of conventional fuel [39]. This strategy reduces the required hydrogen storage, lowering the overall vehicle mass while simultaneously contributing to a reduction in tailpipe emissions [40]. Hydrogen enables the increase of air excess ratios up to two, without substantially prolonging the combustion duration and reducing NO_x emissions. For instance, using a petrol–hydrogen mixture containing 10% hydrogen by mass and increasing the air excess ratio from 1.4 to 1.6 results in only a minor increase in combustion duration, approximately 1–2 degrees of crank angle (CA) [41]. Hydrogen also changes the fraction of carbon-based fuel used, leading to lower emissions of CO, CO_2, and hydrocarbons. Studies have shown that even a small fraction of hydrogen can reduce unburned HC emissions by up to 9% across all load points, including tests conducted at full load, with an additional hydrogen flow of 0.25 kg/h. This reduction is due to the increased combustion speed and improved fuel oxidation by hydrogen, and a rise in combustion temperature [42]. However, while the addition of hydrogen enhances the oxidation of carbon-based fuels, it also influences thermal NO_x formation. The increased combustion temperature caused by hydrogen leads to higher NO_x emissions. Studies have shown that reducing the hydrogen

fraction in the fuel mixture from 15% to 10% decreases NO emissions by 14%, with a further 17% reduction observed when the hydrogen fraction is lowered to 5% [43].

To achieve a more comprehensive evaluation of hydrogen's impact—considering the additional mass of H_2 tanks and driving at different speeds—the WLTP driving simulation will be performed [44,45]. This study is designed to assess the effect of hydrogen as an additive in ICE under energy and performance indicators through experimental investigation and numerical modelling. The rest of this paper is organized as follows: Section 2 describes the materials and methods used for experimental research and numerical simulation. Section 3 discusses the results and comparative analysis based on energy and environmental performance indicators. In Section 4, the conclusions and further research are summarized.

2. Materials and Methods

In the experimental part, engine performance and environmental indicators were analyzed using an engine test bench with different fuels: operating with pure gasoline (labelled G100) in dual-fuel mode (D-F), comprising 95% gasoline by mass and 5% hydrogen by mass (labelled G95H5). In the numerical modelling part, the AVL Cruise™ (Version R2022.2) software was utilized, incorporating data from the experimental tests to perform a numerical simulation WLTC. Fuel consumption and emissions were calculated for both G100 and G95H5 cases.

2.1. Fuel Properties

The main properties of the fuels are presented in Table 1, where the properties of the dual-fuel (D-F) mixture are calculated considering the H_2 mass fraction in the fuel. The lower heating value (LHV) of H_2 is 2.76 times higher compared to G100. Consequently, when 5% H_2 by mass is added to the G95H5 fuel mixture, the energy share of H_2 reaches 12.7%, and the fuel's LHV increases by 6.8%. This indicates that under the same engine load, the cyclic mass of fuel supplied is lower in the G95H5 case. Changes in the elemental composition of the fuel resulted in a 27.9% reduction in the carbon/hydrogen (C/H) ratio and an 8.8% increase in the stoichiometric air/fuel (A/F) mass ratio (which is higher than the increase in the LHV). Consequently, for the same engine load, maintaining a stoichiometric mixture (excess air ratio $\lambda = 1$) with G95H5 required a greater throttle opening due to the increased air demand. The low density and high volumetric displacement of hydrogen in the cylinder further reduce the air intake, necessitating additional throttle opening to maintain $\lambda = 1$. During the WLTC, the required engine power does not reach the maximum specified in the engine design. When operating with G100, the throttle is partially opened, whereas with G95H5, there is room to open the throttle further. However, at maximum throttle opening, the volumetric displacement of hydrogen and the increased air demand for combustion with G95H5 resulted in a smaller cyclic fuel mass compared to G100, leading to a reduction in the engine's maximum brake torque. The significantly reduced C/H ratio of G95H5 suggests lower emissions of CO and CH, as well as reduced greenhouse gas CO_2 during the driving cycle.

Table 1. Key fuel properties [46–48].

Parameter		Gasoline (G100)	Hydrogen ($H_2$100)	D-F (G95H5)	Difference Between D-F G95H5 and G100, %
Density at 15 °C, kg/m^3		736.0	0.09	-	-
Lower heating value *LHV*, MJ/kg		43.53	120.00	47.35	+6.8
Elemental composition, %	C	86.42	0.00	82.10	−5.0
	H	13.58	100.00	17.90	+31.8
C/H		6.36	-	4.59	−27.9
Stoichiometric air–fuel ratio A/F, kg air/1 kg fuel		14.7	35.0	15.7	+8.8

2.2. Experimental Engine Test Bench Equipment

In the first stage of this study, the energy and environmental indicators of a naturally aspirated spark-ignition engine (SIE), the Nissan HR16DE (Nissan Motor Co., Ltd., Yokohama, Japan), were investigated using experimental equipment (Figure 1). According to the engine specifications, it delivers a maximum power output of 84 kW at 6000 rpm. The naturally aspirated engine was equipped with a multi-point fuel injection (MPFI) system operating at 3.5 bar fuel pressure, along with a Continuously Variable Valve Timing Control System (CVTCS). The engine was loaded using the AMX200/100 (Automex, Gdansk, Poland) eddy current engine load stand, which has a torque measurement accuracy of ±0.9 Nm and is capable of applying a maximum torque load of 250 Nm (Table 2).

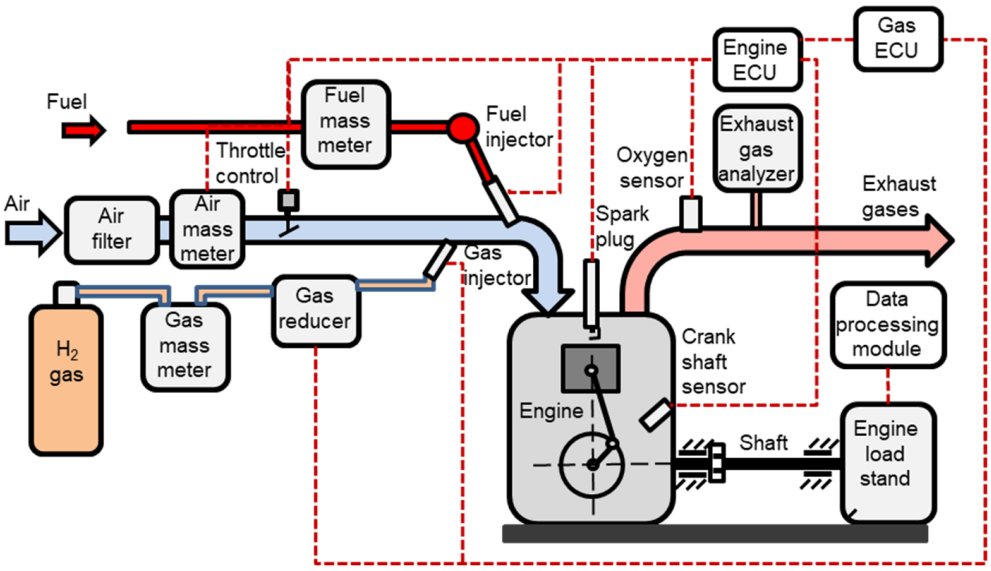

Figure 1. The schematic diagram of the test bench for an SIE under load.

Gasoline consumption was measured using AMX240 (Automex, Gdansk, Poland) gravimetric scales with an accuracy of ±0.10%. Hydrogen consumption was measured using a high-pressure Coriolis mass flow metre RHEONIK RHM 015 (RHEONIK, Odelzhausen, Germany) with an accuracy of ±0.10%. Air mass flow was measured at the intake system using a BOSCH HFM 5 (BOSCH, Stuttgart, Germany) air flow metre, which provides an accuracy of 3%. The composition of the exhaust gasses was analyzed using the AVL DiCOM 4000 (AVL DiTEST, Graz, Austria) gas analyser with the following specifications:

- CO: Measuring range, 0–10% (vol); resolution ±0.01%.
- CO_2: Measuring range, 0–20% (vol); resolution ±0.10%.
- HC: Measuring range, 0–20,000 ppm (vol); resolution ±1 ppm.
- NO_x: Measuring range, 0–4000 ppm (vol); resolution ±1 ppm.
- Excess air ratio (λ): Measuring range, 0–9.999; resolution ±0.001.

In the experimental setup, liquid (G100) and gaseous (H_2) fuels were injected through separate injectors installed in the intake manifold. G100 was injected using the original multi-point injection system of the HR16DE HR16DE (Nissan Motor Co., Ltd., Yokohama, Japan) engine. For injecting hydrogen, a separate multi-point injection system was installed in the intake manifold. To maintain the desired gasoline/hydrogen ratio, the MoTeC M800 (MoTeC, Melbourne, Australia) system was used to adjust the operating ratio of the primary and secondary injectors. The ratio was recalculated based on the mass fuel consumption of G100 and $H_2$100. Engine operating parameters—including throttle position, engine speed, excess air ratio (λ), and ignition timing—were controlled using a programmable electronic engine control unit (ECU), MoTeC M800. A lambda control system maintained a stoichiometric mixture (λ = 1.0) over a wide range of operating conditions. Exceptions occurred at maximum throttle opening, where the mixture was enriched to an excess air ratio of λ = 0.9 to achieve maximum torque. At each measurement point, data were collected five times, and the standard deviation was calculated. If any measurement point showed significant variation, the measurement was repeated.

Table 2. Main parameters of the tested engine.

Parameter	Specification
Engine Type	4 cylinder, DOHC
Displacement	1.6 L (1598 cm^3)
Fuel System	Multi-point fuel injection (MPFI)
Valve Timing	Continuously Variable Valve Timing Control System (CVTCS)
Bore	78.0 mm
Stroke	83.6 mm
Compression Ratio	10.7:1
Block and Head Material	Aluminum alloy
Ignition System	Distributorless ignition system (DIS)
Maximum Power	84 kW (6000 rpm)
Maximum Torque	156 Nm (4400 rpm)
Emissions Compliance	Euro 4

2.3. The Methodology of the Experimental Study on the Engine Load Test Bench

The first stage of the experiments involved testing the engine operation with G100 fuel. Fuel consumption and pollutant concentrations were measured across the full range of engine speeds and loads (Figure 2). The maximum brake torque achieved was 156 Nm. A fuel consumption map (B_{f_G100}, kg/h) was created based on the measured data, illustrating fuel consumption across the operating conditions (Figure 3).

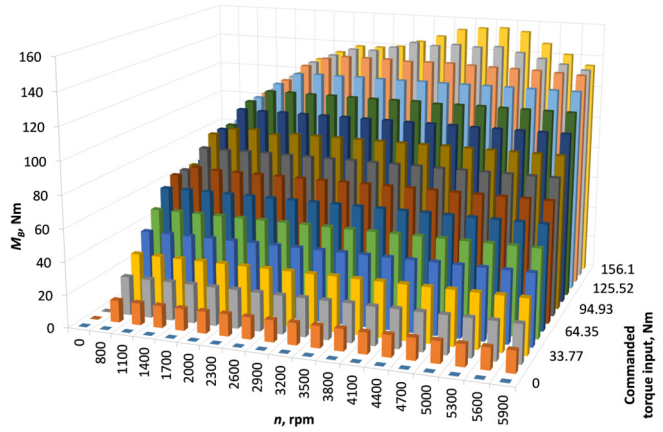

Figure 2. Engine load map.

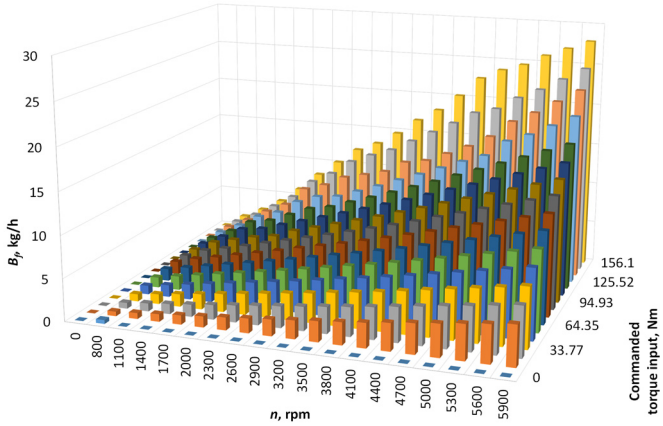

Figure 3. Fuel consumption map for G100.

Before conducting tests with the dual-fuel G95H5 mixture, the gasoline consumption map from the initial G100 testing (B_{f_G100} map, Figure 3) was used to preliminarily calculate the required hydrogen mass flow (5% of G100 by mass). Based on these calculations, a hydrogen consumption map (B_{f_H2}, Figure 4) was created to guide the hydrogen supply during dual-fuel operation. During the dual-fuel experiments, the hydrogen flow specified in the B_{f_H2} map was supplied to the intake manifold through additional gas injectors controlled by the electronically managed OSCAR-N gas injection system. This system received real-time data from the MoTeC M800 ECU, enabling precise synchronization with the gasoline injection system. Gasoline was simultaneously injected via the standard fuel system, with the injector opening duration managed by the MoTeC M800 system. To maintain a stoichiometric mixture ($\lambda = 1.0$), the control system adjusted the gasoline injection volume based on signals from an oxygen sensor installed in the exhaust system. By supplementing the air–gasoline mixture with hydrogen gas (5% of the gasoline mass), while maintaining the same excess air ratio as in the G100 tests, the maximum engine brake torque decreased to 137 Nm, approximately a 12% reduction compared to G100. A dual-fuel consumption map (B_{f_G95H5}, kg/h) was developed (Figure 5). Fuel consumption with G95H5 decreased by approximately 18% compared to G100. This reduction resulted from several complex factors:

1. The low density of hydrogen increases its volumetric displacement, reducing the air intake and thus volumetric efficiency, which decreases torque.
2. G95H5 requires 8.8% more air for combustion compared to G100.
3. The lower heating value (LHV) of the fuel blend increased by 6.8% (Table 1).

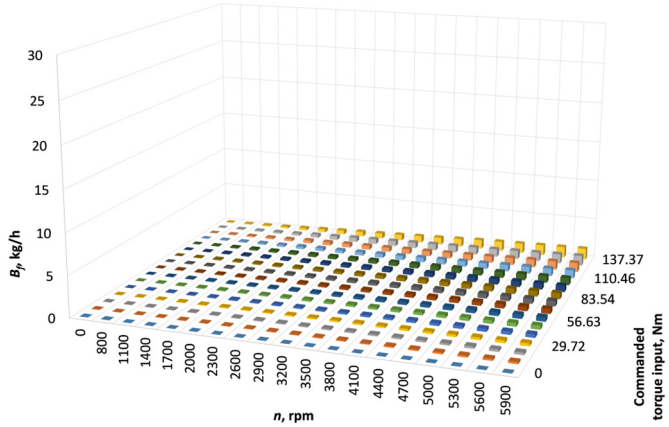

Figure 4. H_2 consumption map.

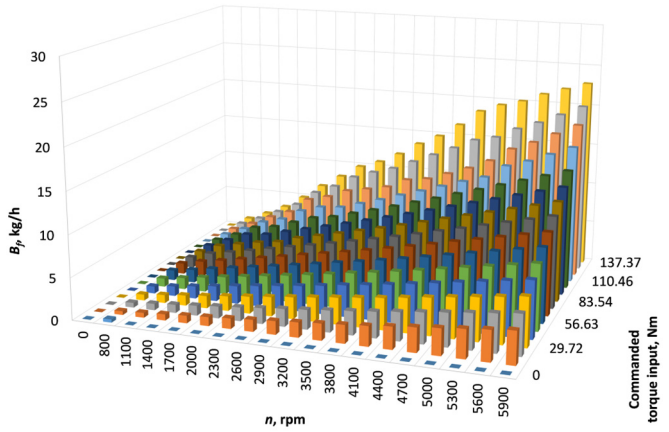

Figure 5. D-F G95H5 consumption map.

The composition of engine exhaust gasses (pollutant concentration) was measured using a stationary gas analyser. Results are given after measuring the pollution before the catalytic converter. The emissions of individual exhaust components were calculated using the specified formulas:

$$E_{CO} = \frac{CO \cdot M_{CO} \cdot m_{ex}}{M_{ex} \cdot 100}, \text{kg/h}; \quad (1)$$

$$E_{CH} = \frac{CH \cdot M_{CH} \cdot m_{ex}}{M_{ex} \cdot 10^6}, \text{kg/h}; \quad (2)$$

$$E_{NO_x} = \frac{NO_x \cdot M_{NO_x} \cdot m_{ex}}{M_{ex} \cdot 10^6}, \text{kg/h}; \quad (3)$$

here, M_{CO}—the molar mass of carbon monoxide, M_{CO} = 28.01 g/mol; CO—the concentration of carbon monoxide in exhaust gasses, %; M_{CH}—the molar mass of unburned hydrocarbons, M_{CH} = 42.5 g/mol; CH—the concentration of unburned hydrocarbons in exhaust gasses, ppm; M_{NO_x}—the molar mass of nitrogen oxides, M_{NO_x} = 30.01 g/mol; NO_x—the concentration of nitrogen oxides in exhaust gasses, ppm; M_{ex}—the molar mass of the exhaust gas mixture, calculated by considering the molar mass of individual exhaust gas components and their concentration in the exhaust gasses, g/mol; m_{ex}—the engine exhaust gas mass emission:

$$m_{ex} = B_f + B_{air}, \text{kg/h}. \quad (4)$$

where B_f—the total mass consumption of gasoline and hydrogen; B_{air}—the air mass consumption.

The load of the SIE was gradually increased to its maximum at various fixed engine speeds. For each measurement point, pollutant emissions were calculated, and pollutant emission maps were created for the engine operating on gasoline and dual fuel. The visualization of CO, CH, and NO_x emissions for the engine operating on D-F G95H5 is presented in Section 3, Results and Discussion.

2.4. The Methodology of WLTC Numerical Simulation

In the second part of this study, to comprehensively evaluate the impact of a hydrogen additive on the performance parameters of a spark-ignition engine operating on gasoline under simulated real-world driving conditions, a numerical model of a Nissan Qashqai J10 (Nissan Motor Co., Ltd., Yokohama, Japan) passenger car was developed using the AVL Cruise™ simulation software (Figure 6). The vehicle is equipped with a four-cylinder spark-ignition engine (HR16DE) with a displacement of 1.598 dm^3, a maximum power output of 84 kW at 6000 rpm, and a maximum brake torque of 156 Nm at 4400 rpm. The vehicle's wheelbase length is 2630 mm, the frontal surface area is 2.32 m^2, the aerodynamic drag coefficient is 0.32, the curb weight is 1272 kg, and the maximum allowable weight is 1830 kg. The car features a five-speed manual transmission with the following gear ratios: 3.73, 2.1, 1.39, 1.09, and 0.89. The capacity of the fuel tank is 65 L, and the dimensions of the tires of 215/65 R16 are used in this model.

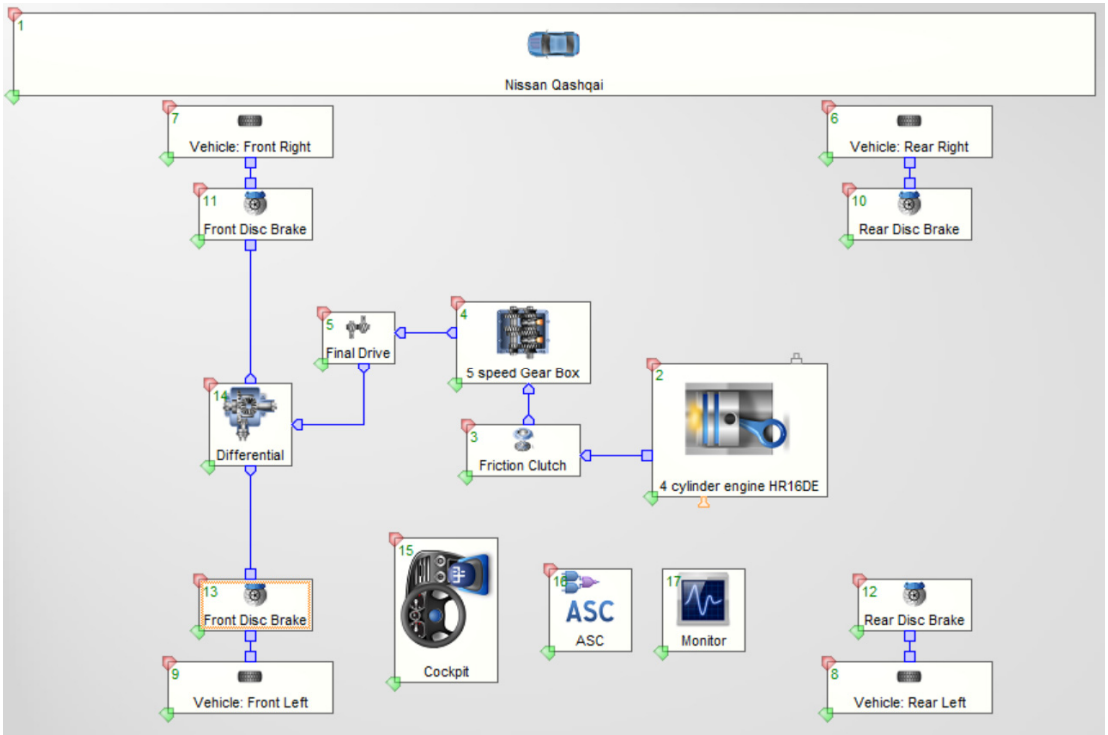

Figure 6. The numerical model of the Nissan Qashqai J10 vehicle in AVL Cruise™ simulation software: 1—the main vehicle component Nissan Qashqai, 2—the naturally aspirated internal combustion engine HR16DE, 3—friction clutch, 4—manual transmission, 5—final drive, 6—rear right wheel, 7—front right wheel, 8—rear left wheel, 9—front left wheel, 10—rear right brake disc, 11—front right brake disc, 12—rear left brake disc, 13—front left brake disc, 14—differential, 15—cockpit, 16—anti-slip control (ASC) system, and 17—monitor.

According to the Worldwide Harmonised Light Vehicles Test Procedure (WLTP), based on the engine power-to-mass ratio (PMR) and the manufacturer-declared maximum vehicle speed, the WLTC driving cycle was assigned to "Class 3b". Vehicles in "Class 3b" have an engine power-to-mass ratio greater than 34 W/kg and a manufacturer-declared maximum

speed of at least 120 km/h. The tested vehicle's maximum speed is 175 km/h, and its PMR is 66.04 W/kg.

The WLTC simulation task for the vehicle was created in a dedicated folder within the simulation software by inputting the driving cycle data (time–speed–load). During the numerical simulation, real-world driving conditions were modelled for 30 min across four distinct modes:

1. Urban cycle: a maximum speed of up to 56.5 km/h, average speed of 18.9 km/h, duration of 589 s, and distance of 3.09 km.
2. Medium-speed cycle: a maximum speed up of to 76.6 km/h, average speed of 39.5 km/h, duration of 433 s, and distance of 4.76 km.
3. High-speed cycle: a maximum speed of up to 97.4 km/h, average speed of 56.7 km/h, duration of 455 s, and distance of 7.16 km.
4. Very high-speed cycle: a maximum speed of up to 131.3 km/h, average speed of 92 km/h, duration of 323 s, and distance of 8.25 km.

Environmental conditions during the simulation were set as follows: an ambient temperature of 23 °C, relative humidity of 50%, and atmospheric pressure of 1.013 bar.

As shown in Figure 7, during the WLTC simulation conducted using AVL Cruise™, the tested vehicle travelled a total distance of 23.27 km in 1800 s while maintaining the prescribed speeds. An analogous driving cycle was simulated with the vehicle operating on both G100 and G95H5 fuels.

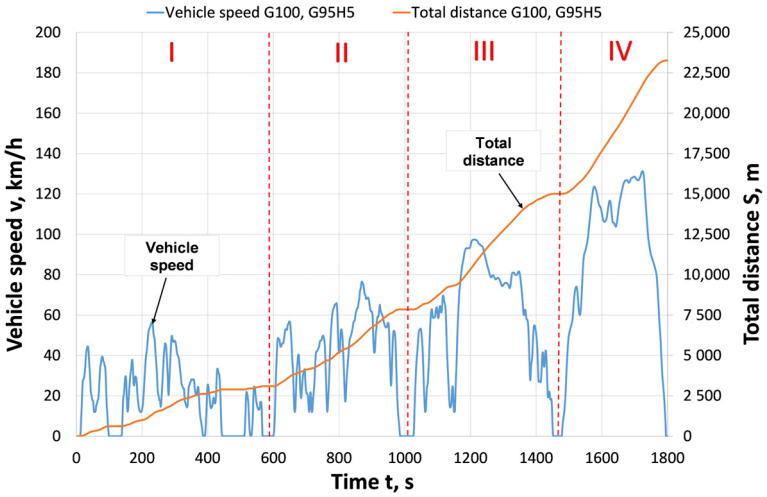

Figure 7. The vehicle speed v and distance S travelled in the WLTC simulation: I—Urban cycle; II—Medium-speed cycle; III—High-speed cycle; IV—Very high-speed cycle.

In this study, the vehicle's WLTC was simulated using the AVL Cruise™ software. In the near future, after installing an additional hydrogen fuelling system in the vehicle, real-world driving tests are planned. The experimental investigation of the WLTC cycle will involve the use of a chassis dynamometer, fuel (gasoline and hydrogen) mass metre, air mass metre, gas analyser, and other equipment. Using data obtained from the experimental tests, the vehicle's energy and environmental performance indicators will be calculated [49], and the validation of the numerical simulation results presented in this article will be conducted. During the WLTC experimental tests on the chassis dynamometer, the spark-ignition engine (SIE) will operate under various transient modes. These operational parameters may not fully match the results obtained during the simulation, as the latter relied on experimental data measured under stable engine operating conditions.

3. Results and Discussion

In the second stage of this study, using data from the Nissan Qashqai J10 vehicle, the AVL Cruise™ program was used to calculate the engine speed (Figure 8), brake torque (Figure 9), and power (Figure 10) at all WLTC driving points. The engine speed was calculated while driving in the following modes: urban cycle (I), average speed (II), and high speed (III) range from 1700 to 3800 rpm, depending on the vehicle speed and the selected gear. When driving at very high speeds (IV), the engine speed increases to 2500–4500 rpm, as the highest gear in the gearbox is five, and this gear is engaged when the vehicle speed reaches 80–90 km/h. Increasing the vehicle speed from 80 km/h to 130 km/h does not allow for a reduction in the gear ratio, and the engine speed increases by approximately 1.6 times. Replacing fuel G100 with G95H5 causes only a slight change in engine speed, as the gears are shifted identically in both cases. Engine speed is one of the coordinates in the fuel consumption and pollutant emission maps used to select the necessary parameters for WLTC indicator calculations.

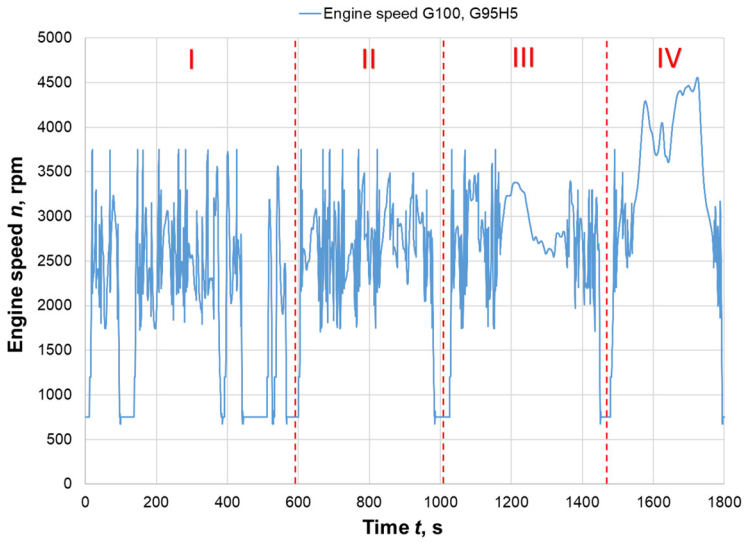

Figure 8. Internal combustion engine speed n during WLTC simulation: I—Urban cycle; II—Medium-speed cycle; III—High-speed cycle; IV—Very high-speed cycle.

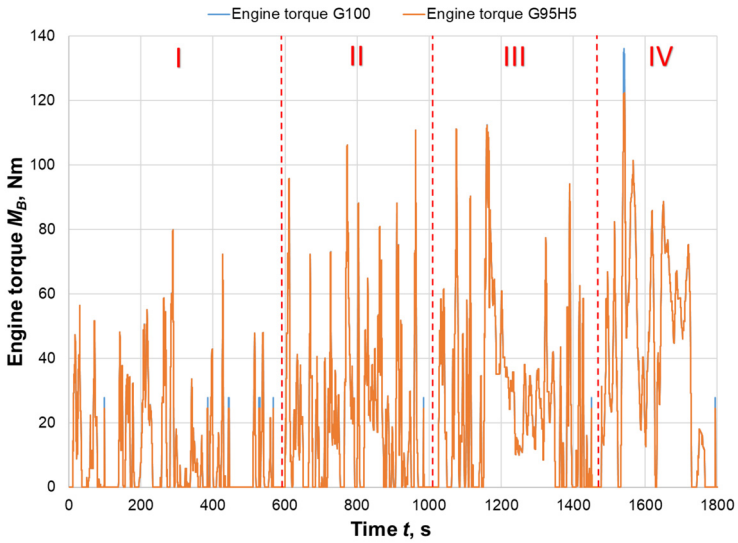

Figure 9. The brake torque M_B of the internal combustion engine during WLTC simulation: I—Urban cycle; II—Medium-speed cycle; III—High-speed cycle; IV—Very high-speed cycle.

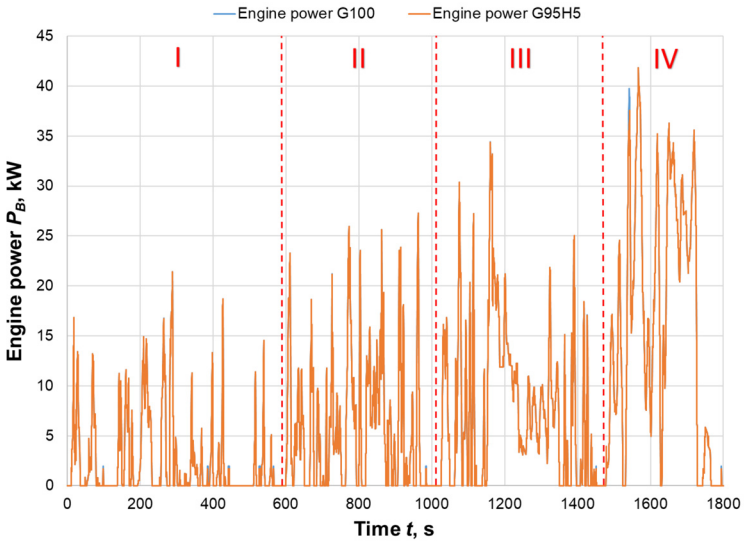

Figure 10. The brake power P_B of the internal combustion engine during WLTC simulation: I—Urban cycle; II—Medium-speed cycle; III—High-speed cycle; IV—Very high-speed cycle.

The SIE brake torque dynamically varies at all WLTC points (Figure 9), which confirms that the engine operates in transitional modes during real driving. The load, in particular, increases as the vehicle accelerates and overcomes inertia, with the maximum value when driving at high and very high speeds approaching 140 Nm. Engine load is the second coordinate used for selecting the necessary parameters for the WLTC indicator calculations.

The engine brake power directly depends on the engine speed and brake torque, and throughout the entire WLTC period, it fluctuates (Figure 10). The engine's effective power is zero when the engine is idling, or engine braking is occurring. When the vehicle is travelling at a high speed of 130 km/h, the engine load power ranges between 20 and 35 kW. During rapid acceleration, the power demand reaches 45 kW, and the engine still has a ~45 kW reserve. Whether the vehicle is powered by G100 or G95H5 fuel, the engine brake power values at all WLTC points are similar, as the fuel type has minimal impact on engine load. The only significant influence is the increased vehicle mass due to the additional hydrogen supply system.

In the WLTC test stage, the fuel consumption B_f data (maps) for the engine operating on G100 and G95H5 fuels (Figures 3 and 5) were uploaded into the AVL Cruise™ numerical simulation program. These maps were created based on the authors' preliminary experimental studies and the results of other studies [50–52]. When analyzing the instantaneous fuel consumption determined through numerical modelling, lower consumption values for G95H5 are visually observed (Figure 11). After calculating the total fuel consumption during WLTC, the fuel consumption for G100 and G95H5 was found to be 1.03 kg (44.92 MJ) and 0.92 kg (43.76 MJ), respectively. The reduction of approximately 10.4% in dual-fuel G95H5 consumption compared to G100 was due to a 6.8% higher D-F LHV (Table 1) and increased brake thermal efficiency due to the hydrogen addition. An evaluation of fuel consumption during WLTC and LHV showed that replacing G100 with G95H5 reduced fuel energy consumption by about 2.57%. The thermal efficiency of combustion increased, as hydrogen accelerated and improved the combustion process, which reduced energy loss through exhaust gasses and increased energy release due to more complete combustion. These results are consistent with other researchers [50,53,54].

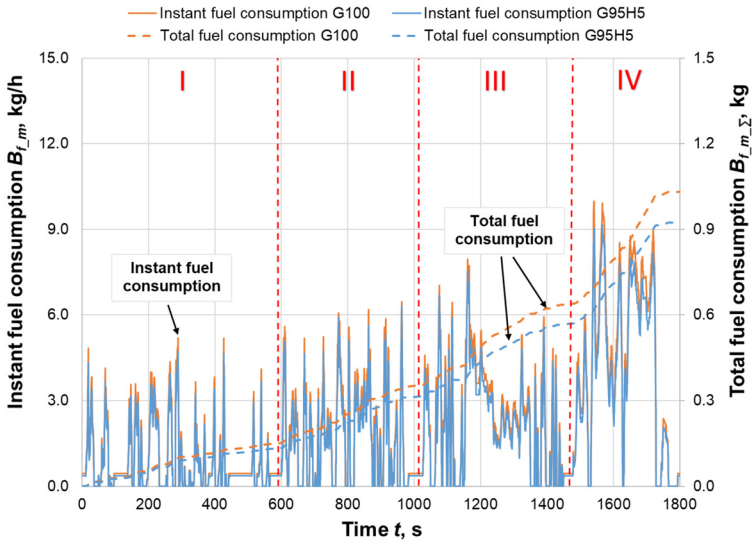

Figure 11. Fuel consumption during the WLTC test using pure gasoline G100 and dual-fuel G95H5: I—Urban cycle; II—Medium-speed cycle; III—High-speed cycle; IV—Very high-speed cycle.

The emission indicators of an SIE (E_{CO}, E_{HC}, and E_{NO_x}) using G100 and G95H5 fuels (Figures 12–14) across a wide range of engine speeds and loads were determined in the first stage of the study through experimental engine testing on a dynamometer. The emission trends of incomplete combustion products (CO and HC) and nitrogen oxides varied with changes in engine load and speed, but certain similarities were also observed. At low and moderate loads and speeds, CO emissions were relatively low due to the maintenance of stoichiometric air excess, ensuring efficient combustion (Figure 12). As engine loads approached maximum levels, the mixture was enriched, leading to a significant increase in CO emissions, especially at maximum speeds, as combustion time decreased. HC emissions consistently increased with rising engine speed and load (Figure 13) due to the greater amount of combustible mixture in the cylinder and the reduced combustion duration. Similarly to the case of CO, a sharp increase in HC emissions was observed when approaching maximum torque, and the air–fuel mixture was enriched [55].

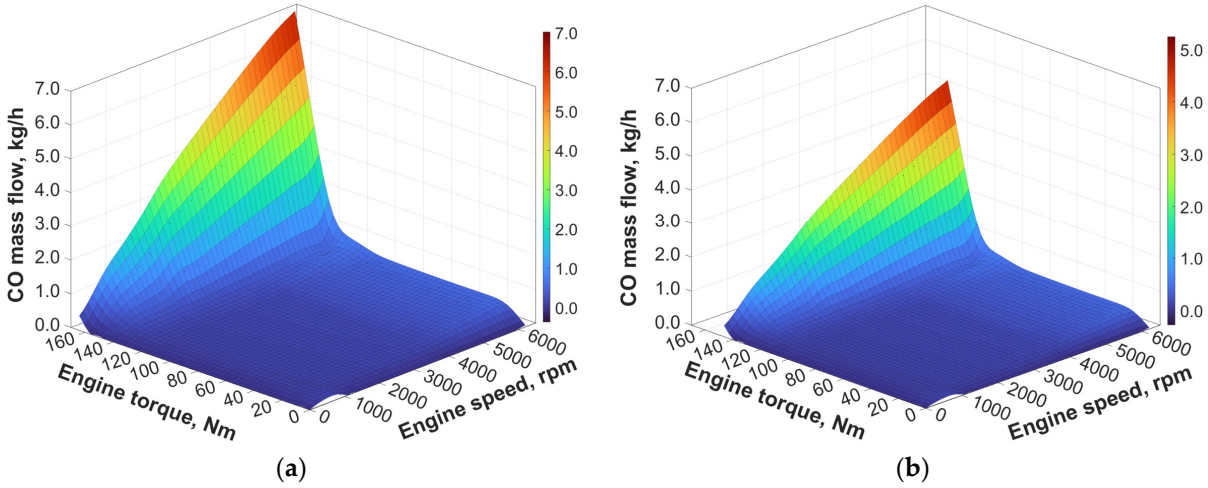

Figure 12. CO emissions map: (**a**) G100; (**b**) G95H5.

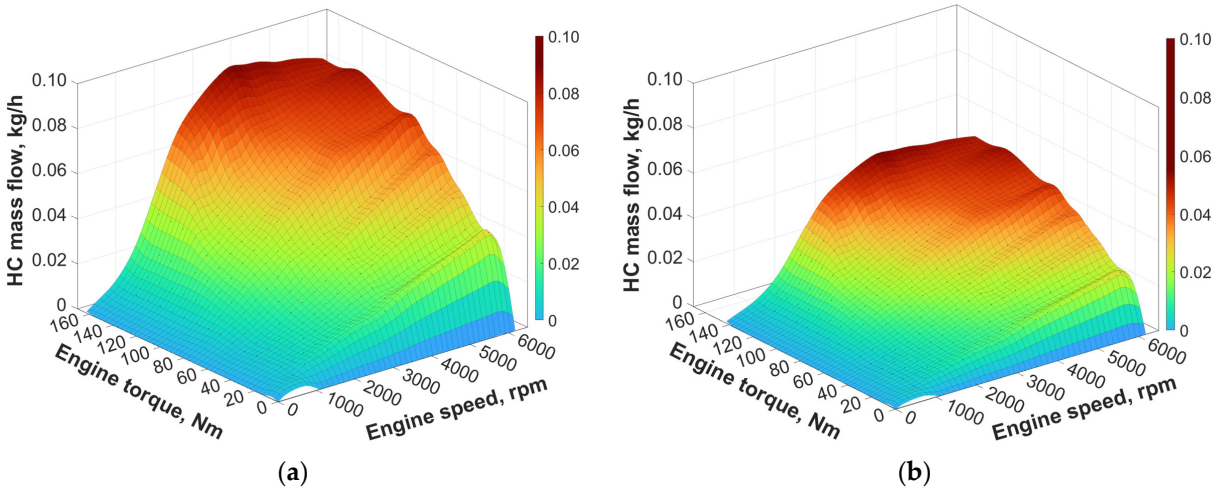

Figure 13. HC emissions map: (**a**) G100; (**b**) G95H5.

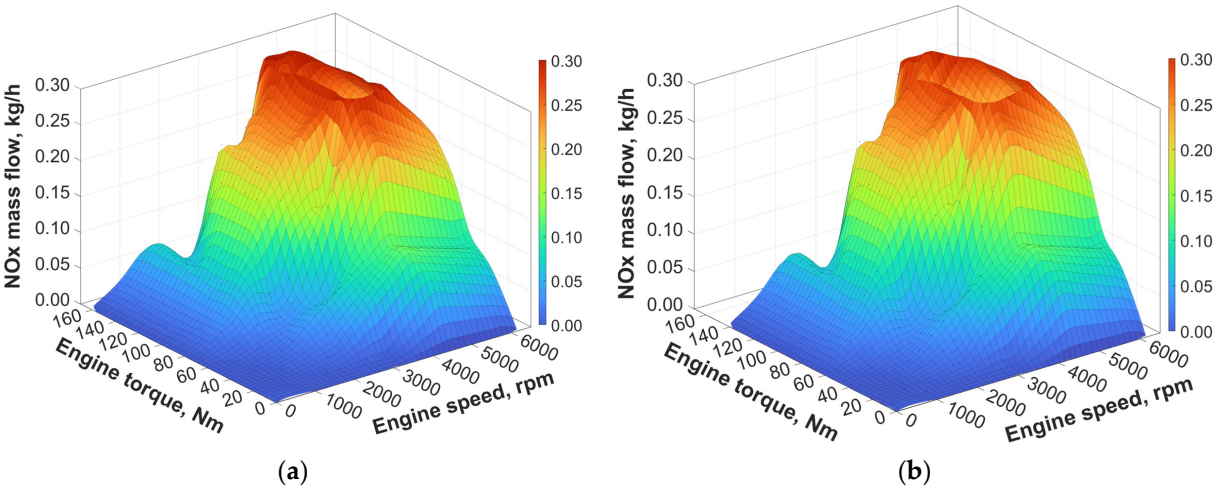

Figure 14. NO_x emissions map: (**a**) G100; (**b**) G95H5.

The NO_x emissions were determined by the combustion temperature in the cylinder and the air excess coefficient. It was observed that increasing the engine load resulted in a rise in NO_x emissions (Figure 14). This was due to the greater volume of the air–fuel mixture in the cylinder (volumetric efficiency) caused by a wider throttle opening, which increased the combustion temperature in the cylinder. However, as engine loads approached maximum levels, a significant increase in NO_x emissions (as seen in the cases of CO and HC) did not occur due to the richer fuel mixture and a lack of oxygen [54,56].

In the second stage of the research, the engine emission data (E_{CO}, $E_{HC,}$ and E_{NO_x}) were uploaded into the AVL Cruise™ numerical simulation software and used to determine the vehicle's emissions at individual WLTC points (instant emissions), based on specific engine speeds and loads. These point-specific emission data were then used to calculate the total emissions over the entire test cycle. Several researchers have published similar studies, but they used gas rather than petrol [57,58].

Figures 15 and 16 show quite different trends in the emissions of incomplete combustion products (CO and HC). This is due to the different tendency observed in the CO and HC emission maps (Figures 12 and 13). The total emissions (kg) calculated using the AVL Cruise software were used to analyze the specific emissions (g/km) of the different driving phases (cycles) of the WLTC by dividing the total emissions by the distance travelled during driving mode. During the urban cycle (I), the CO specific emissions were low (0.38 g/km

for G100 and 0.30 g/km for G95H5) but increased significantly (~8 times) with increased engine load and the enrichment of the air–fuel mixture (3.0 g/km for G100 and 2.3 g/km for G95H5) at very high vehicle speeds (IV). The HC specific emission intensity at low load (I) is even slightly higher (0.85 g/km for G100 and 0.54 g/km for G95H5) compared to very high vehicle speeds (IV) (0.46 g/km for G100 and 0.30 g/km for G95H5), due to the fact that combustion is carried out at a lower temperature at low load, and therefore, the HC emissions are still high, even at idling speed.

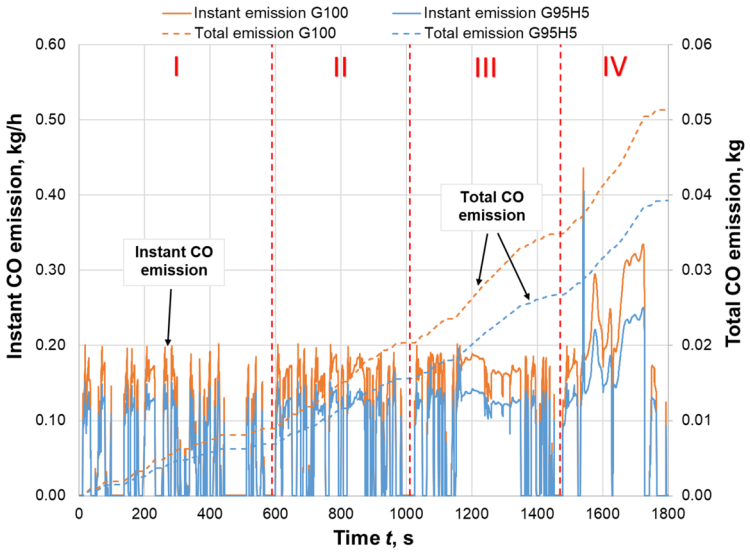

Figure 15. Instant and total CO emissions during the WLTC test: I—Urban cycle; II—Medium-speed cycle; III—High-speed cycle; IV—Very high-speed cycle.

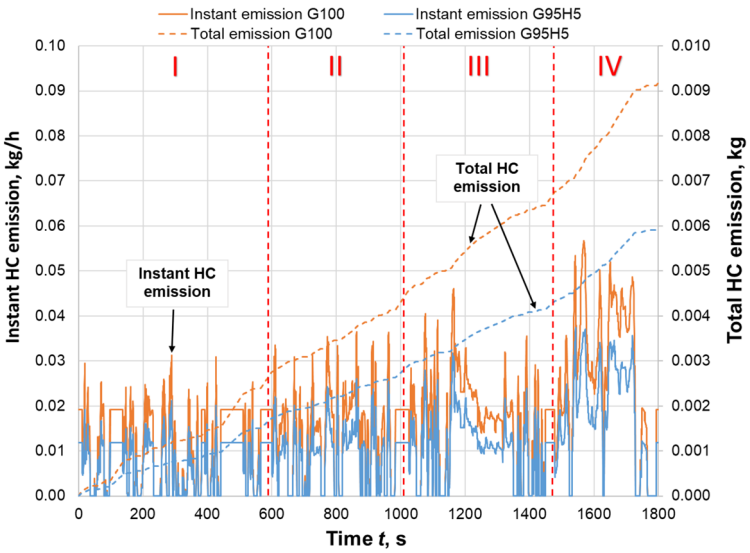

Figure 16. Instant and total HC emissions during the WLTC test: I—Urban cycle; II—Medium-speed cycle; III—High-speed cycle; IV—Very high-speed cycle.

When analyzing carbon monoxide (CO) emission trends over the WLTC using G100 and G95H5 fuels, the addition of 5% hydrogen by mass to gasoline significantly reduced cumulative CO emissions. This reduction was attributed to the altered fuel composition and more efficient combustion process. The hydrogen additive decreased the C/H ratio in the fuel mixture by 27.9% and increased the combustion rate. In city driving conditions (Phase I), the total CO emissions reached 8.9 g for G100 and 6.9 g for G95H5, representing a 22.9% reduction in total emissions. As the vehicle transitioned to suburban conditions (medium-

speed regime) in Phase II, hydrogen reduced the total CO emissions by 23.6%. After the first two WLTC phases, the total CO emissions reached 20.3 g for G100 and 15.6 g for G95H5. During rural conditions (high-speed regime) in Phase III, numerical simulation determined that the hydrogen additive reduced CO emissions by 23.4%, with cumulative CO emissions after the first three phases reaching 34.9 g for G100 and 26.7 g for G95H5. In Phase IV, during highway conditions (very high-speed regime), aerodynamic drag increased fuel consumption, leading to the most intense growth in CO emissions. In this phase, a 23.9% reduction in CO emissions due to hydrogen was observed. The total CO emissions after all four WLTC driving phases amounted to 51.3 g for G100 and 39.2 g for G95H5, reflecting a 23.6% decrease. The greater effect of hydrogen in reducing CO emissions was achieved when the engine operated dynamically, under higher loads, and with a richer air–fuel mixture. The specific CO emissions for individual WLTC driving phases using G100 and G95H5 fuels were as follows: Phase I: 0.384 g/km (G100) vs. 0.296 g/km (G95H5), Phase II: 2.57 g/km (G100) vs. 1.97 g/km (G95H5), Phase III: 2.34 g/km (G100) vs. 1.79 g/km (G95H5), and Phase IV: 3.04 g/km (G100) vs. 2.32 g/km (G95H5). Considering the total WLTC driving distance of 23.27 km, the calculated specific CO emissions were 2.21 g/km for G100 and 1.69 g/km for G95H5. The tested vehicle must comply with the Euro 4 emission standard, which permits a maximum CO emission level of 1.0 g/km. This study evaluated emissions before the catalytic converter. With the use of a catalytic converter, CO emissions would be significantly reduced, and for both fuels, they would meet the standard requirements.

The addition of 5% hydrogen to gasoline during the WLTC significantly reduced total HC emissions in all driving conditions. In city driving conditions (Phase I), the hydrogen additive reduced total HC emissions by 37.1%, from 2.65 g (G100) to 1.66 g (G95H5) (Figure 16). During suburban conditions (Phase II), the reduction in cumulative HC emissions with hydrogen was 36.5%, with total HC emissions after the first two phases reaching 4.54 g for G100 and 2.89 g for G95H5. In rural conditions (Phase III), hydrogen reduced HC emissions by 35.2%, with cumulative HC emissions after three phases totaling 6.75 g for G100 and 4.32 g for G95H5. During highway conditions (Phase IV), where increased aerodynamic drag raised fuel consumption, the hydrogen additive reduced HC emissions by 34.1%. After all four WLTC phases, the total HC emissions were 9.19 g for G100 and 5.95 g for G95H5, resulting in a 35.2% decrease in HC emissions across the full driving cycle. The specific HC emissions for individual WLTC phases using G100 and G95H5 fuels were as follows: Phase I: 0.853 g/km (G100) vs. 0.537 g/km (G95H5), Phase II: 0.617 g/km (G100) vs. 0.391 g/km (G95H5), Phase III: 0.405 g/km (G100) vs. 0.262 g/km (G95H5), and Phase IV: 0.455 g/km (G100) vs. 0.300 g/km (G95H5). This analysis shows that HC emissions were of similar intensity across all driving phases. The positive effect of the hydrogen additive was more pronounced in the initial WLTC driving phases, where engine loads were lower. This improved HC combustion at lower combustion temperatures, differing from the trend observed in CO emission reductions with hydrogen. The specific HC emissions over the full WLTC were calculated at 0.395 g/km for G100 and 0.256 g/km for G95H5. The tested vehicle is certified to meet the Euro 4 emission standard, which allows a maximum HC emission level of 0.1 g/km. With the use of a catalytic converter, HC emissions would be significantly reduced and would meet the ecological requirements for both fuels.

Numerical modelling using the AVL Cruise™ software shows that a 5% hydrogen additive in gasoline has a varying impact on NO_x emissions across different WLTC phases. At the end of the city driving cycle (Phase I), the total NO_x emissions were 2.0 g for G100 and 2.46 g (22.7% higher) for G95H5 (Figure 17), with specific emissions of 0.647 g/km and 0.794 g/km, respectively. In the medium-speed regime (Phase II), NO_x emissions

increased due to higher engine loads, with hydrogen further increasing NO_x emissions by 25.9%. Specific emissions rose to 0.787 g/km for G100 and 0.991 g/km for G95H5, resulting in total emissions of 5.6 g for G100 and 7.0 g for G95H5 after two phases. In the high-speed regime (Phase III), the impact of hydrogen on NO_x emissions remained significant, increasing emissions by 23.5%. Specific emissions reached 0.897 g/km for G100 and 1.108 g/km for G95H5, with total NO_x emissions after three phases amounting to 11.3 g for G100 and 14.0 g for G95H5. During the very high-speed regime (Phase IV), higher engine loads and elevated combustion temperatures in the cylinder resulted in substantially higher NO_x emissions. Specific emissions in this phase reached 1.714 g/km for G100, while the hydrogen additive increased NO_x emissions by 19.7%, raising specific emissions to 2.051 g/km for G95H5. At the end of the WLTC, the total NO_x emissions were 22.7 g for G100 and 27.6 g for G95H5, representing a 21.4% increase due to hydrogen. An analysis of individual cycle phases indicates that the hydrogen additive had the greatest impact on NO_x emissions during Phases II and III, which involved more accelerations and higher engine loads. Over the full WLTC, the specific NO_x emissions were 0.978 g/km for G100 and 1.187 g/km for G95H5. The Euro 4 emission standard allows a maximum NO_x emission of 0.08 g/km. It is expected that with the use of a catalytic converter, this standard will be met.

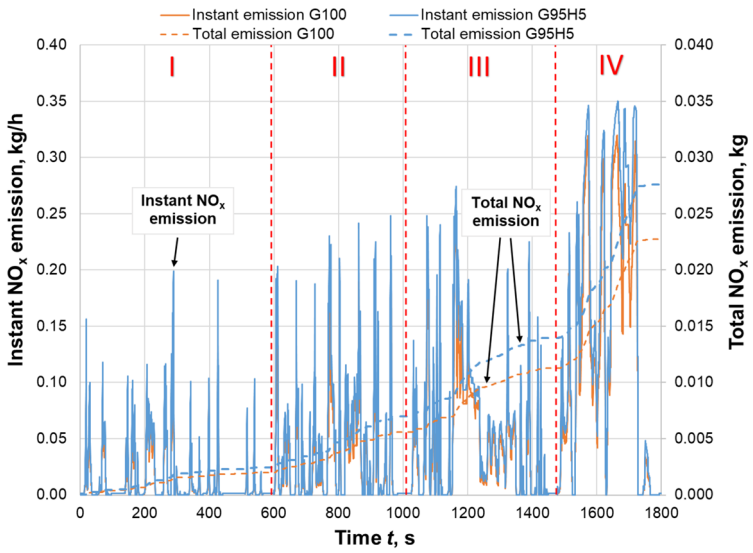

Figure 17. Instant and total NO_x emissions during the WLTC test: I—Urban cycle; II—Medium-speed cycle; III—High-speed cycle; IV—Very high-speed cycle.

The AVL Cruise™ software calculated CO_2 emissions over the WLTC by evaluating the elemental fuel composition and fuel consumption (Figure 18). The addition of 5% hydrogen by mass to gasoline reduced fuel consumption by approximately 10.4%, due to increased engine brake thermal efficiency and a 6.8% higher lower heating value of the fuel (Table 1). This hydrogen additive led to a 5% reduction in the elemental carbon content of the fuel (Table 1), which collectively contributed to a decrease in greenhouse gas CO_2 emissions. In the city driving mode (Phase I), total CO_2 emissions were 476 g for G100 and 399 g for G95H5 (16.1% less), with specific CO_2 emissions of 154 g/km for G100 and 129 g/km for G95H5, respectively. In the medium-speed mode (Phase II), specific CO_2 emissions decreased to 135 g/km for G100 and 115 g/km for G95H5 (15.3% less), and at the end of this phase, total CO_2 emissions were 1.119 kg for G100 and 0.994 kg for G95H5. In the high-speed mode (Phase III), fuel consumption per kilometre and specific CO_2 emissions were at their lowest—126 g/km for G100 and 107 g/km for G95H5 (14.9% less), with total CO_2 emissions at the end of this phase reaching 2.017 kg for G100 and 1.708 kg for G95H5.

In the very high-speed mode (Phase IV), specific CO_2 emissions increased to 150 g/km for G100 and 128 g/km for G95H5 (14.4% less), and by the end of the WLTC, total CO_2 emissions were 3.254 kg for G100 and 2.768 kg for G95H5.

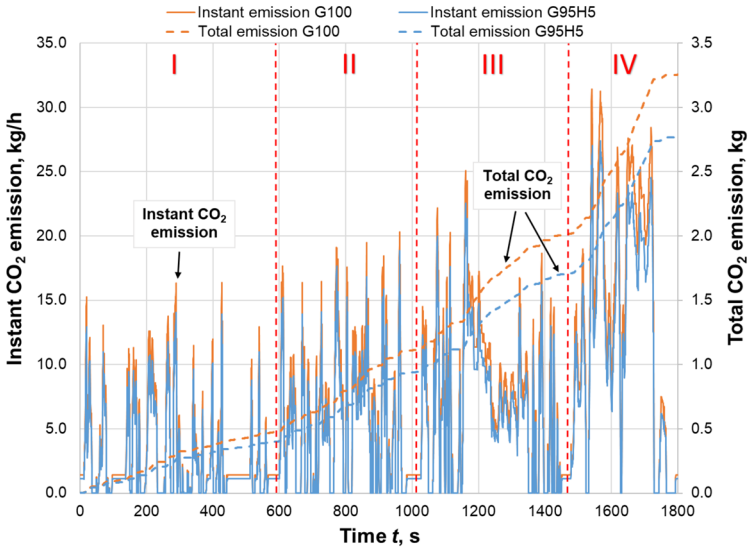

Figure 18. Instant and total CO_2 emissions during the WLTC test: I—Urban cycle; II—Medium-speed cycle; III—High-speed cycle; IV—Very high-speed cycle.

It was calculated that the specific emissions over the WLTC were 140 g/km for G100 and 119 g/km for G95H5 (14.9% lower). According to the European Parliament and Council regulation, each car manufacturer is required to achieve a CO_2 specific emission target of 95 g/km by 2021 [59,60]. The AVL Cruise™ software's results for the CO_2 emissions of the Nissan Qashqai J10 show that with pure gasoline, this target cannot be reached. The 5% hydrogen additive significantly reduced CO_2 emissions, but additional measures are required to meet the target. These could include replacing gasoline with renewable fuels that have a lower C/H ratio, as well as increasing the hydrogen concentration in the dual-fuel mixture. To determine the pollutant and CO_2 emission results using new fuels, further detailed experimental and numerical modelling studies will be needed.

4. Conclusions

The numerical WLTC simulation using the AVL Cruise™ software was conducted for a Nissan Qashqai J10 passenger car equipped with a 1.6 L spark-ignition engine operating on pure gasoline (G100) or dual fuel (D-F) consisting of 95% (by mass) gasoline and 5% hydrogen (G95H5). Real vehicle data, fuel properties, and engine experimental research data (fuel consumption, CO, HC, and NO_x emissions maps) were utilized for the WLTC simulation. Through numerical simulation, the indicators of fuel consumption and pollutant emissions were determined for the vehicle operating under four driving modes: urban cycle (I), medium speed (II), high speed (III), and very high speed (IV).

1. The addition of 5% hydrogen reduced overall fuel mass consumption by about 10% (primarily due to a higher LHV and a roughly 2.57% increase in thermal efficiency).
2. CO and HC emissions decreased significantly (up to 23.9% and 37.1%, respectively, depending on the driving mode), owing to faster combustion and better efficiency. However, NO_x emissions increased (by 19.7% in mode IV and by 25.9% in mode II) due to higher combustion temperatures and more intense heat release. Reduced carbon content (by 5%) and lower fuel consumption cut CO_2 emissions by 14.9% compared to pure gasoline. Despite this reduction, the WLTC simulation showed CO_2 levels remain above the EU's 95 g/km target.

3. Blending gasoline with biofuels (e.g., bioethanol, biobutanol) and/or increasing hydrogen concentration in the fuel are potential pathways to further emission reductions and compliance with stricter EU standards.

To meet EU emission standards, further research is planned, focusing on the use of gasoline and biofuel blends (such as bioethanol, biobutanol, etc.) and increasing the hydrogen concentration in dual fuels.

Author Contributions: Conceptualization, S.P. and A.R.; methodology, A.R. and G.M.; software, T.V. and A.U.; validation, T.V., A.U. and G.M.; formal analysis, S.S. and R.J.; investigation, A.R., T.V. and G.M.; resources, J.Ž., A.U., V.M. and V.Ž.; data curation, T.V., V.Ž. and A.N.; writing—original draft preparation, A.R. and T.V.; writing—review and editing, D.K. and S.S.; visualization, A.R., V.M. and T.V.; supervision, A.R.; project administration, S.P. All authors have read and agreed to the published version of the manuscript.

Funding: Research was conducted as part of the execution of Project "Mission-driven Implementation of Science and Innovation Programmes" (No. 02-002-P-0001), funded by the Economic Revitalization and Resilience Enhancement Plan "New Generation Lithuania".

Institutional Review Board Statement: Not applicable.

Informed Consent Statement: Not applicable.

Data Availability Statement: The data presented in this study are available on request from the corresponding author.

Acknowledgments: A part of the results included in this study have been obtained using internal engine simulation software AVL Cruise™ acquired by signing a Cooperation Agreement between AVL Advanced Simulation Technologies and the Faculty of Transport Engineering of Vilnius Gediminas Technical University.

Conflicts of Interest: The authors declare no conflicts of interest.

Abbreviations

A/F	air/fuel mass ratio
B_f	hourly fuel consumption
CA	crank angle
CAD	crank angle degrees
CH_4	methane
C/H	carbon/hydrogen ratio
CO	carbon monoxide
CO_2	carbon dioxide
D-F	dual fuel
ECU	engine control unit
EU 27	27 member states of the European Union
ICE	internal combustion engine
GDP	gross domestic product
GHGs	greenhouse gasses
G100	pure gasoline
G95H5	hydrogen additive, constituting 5% of the gasoline mass
HC	hydrocarbons
H_2	hydrogen
H_2O	water vapour
$H_2$100	pure hydrogen
SIE	spark-ignition engine
LHV	lower heating value

$MtCO_2e$	million metric tons of carbon dioxide equivalent
NO_x	nitrogen oxides
N_2O	nitrous oxide
PM	particulate matter
PMR	power-to-mass ratio
WLTC	Worldwide Harmonised Light Vehicles Test Cycle
λ	excess air ratio

References

1. Crippa, M.; Guizzardi, D.; Schaaf, E.; Monforti-Ferrario, F.; Quadrelli, R.; Risquez Martin, A.; Rossi, S.; Vignati, E.; Muntean, M.; Brandao De Melo, J.; et al. *GHG Emissions of All World Countries: 2023*; Publications Office of the European Union: Luxembourg, 2023; ISBN 978-92-68-07550-0.
2. Kazancoglu, Y.; Ozbiltekin-Pala, M.; Ozkan-Ozen, Y.D. Prediction and Evaluation of Greenhouse Gas Emissions for Sustainable Road Transport within Europe. *Sustain. Cities Soc.* **2021**, *70*, 102924. [CrossRef]
3. Ji, T.; Li, K.; Sun, Q.; Duan, Z. Urban Transport Emission Prediction Analysis through Machine Learning and Deep Learning Techniques. *Transp. Res. Part Transp. Environ.* **2024**, *135*, 104389. [CrossRef]
4. Jin, Y.; Sharifi, A.; Li, Z.; Chen, S.; Zeng, S.; Zhao, S. Carbon Emission Prediction Models: A Review. *Sci. Total Environ.* **2024**, *927*, 172319. [CrossRef]
5. Khalil, M.; AlSayed, A.; Elsayed, A.; Sherif Zaghloul, M.; Bell, K.Y.; Al-Omari, A.; Laqa Kakar, F.; Houweling, D.; Santoro, D.; Porro, J.; et al. Advances in GHG Emissions Modelling for WRRFs: From State-of-the-Art Methods to Full-Scale Applications. *Chem. Eng. J.* **2024**, *494*, 153053. [CrossRef]
6. Dolge, K.; Blumberga, D. Economic Growth in Contrast to GHG Emission Reduction Measures in Green Deal Context. *Ecol. Indic.* **2021**, *130*, 108153. [CrossRef]
7. European Climate Law—European Commission. Available online: https://climate.ec.europa.eu/eu-action/european-climate-law_en (accessed on 21 December 2024).
8. State of the Union: Commission Raises Climate Ambition. Available online: https://ec.europa.eu/commission/presscorner/detail/en/ip_20_1599 (accessed on 21 December 2024).
9. Abdul-Manan, A.F.N. Uncertainty and Differences in GHG Emissions between Electric and Conventional Gasoline Vehicles with Implications for Transport Policy Making. *Energy Policy* **2015**, *87*, 1–7. [CrossRef]
10. Statista EU-27: GHG Emissions Breakdown by Sector. Available online: https://www.statista.com/statistics/1325132/ghg-emissions-shares-sector-european-union-eu/ (accessed on 17 December 2024).
11. Foretich, A.; Zaimes, G.G.; Hawkins, T.R.; Newes, E. Challenges and Opportunities for Alternative Fuels in the Maritime Sector. *Marit. Transp. Res.* **2021**, *2*, 100033. [CrossRef]
12. IRENA Hydrogen A Renewable Energy Perspective. Available online: https://www.irena.org/publications/2019/Sep/Hydrogen-A-renewable-energy-perspective (accessed on 17 December 2024).
13. Gao, W.; Fu, Z.; Li, Y.; Li, Y.; Zou, J. Progress of Performance, Emission, and Technical Measures of Hydrogen Fuel Internal-Combustion Engines. *Energies* **2022**, *15*, 7401. [CrossRef]
14. Stępień, Z. A Comprehensive Overview of Hydrogen-Fueled Internal Combustion Engines: Achievements and Future Challenges. *Energies* **2021**, *14*, 6504. [CrossRef]
15. Jacquemin, J.; Thiran, P.; Quoilin, S. Prioritizing the Role of Renewable Fuels and Hydrogen Networks in the Transition towards Net Zero Emissions in Western Europe. *Energy* **2025**, *314*, 134069. [CrossRef]
16. Batgi, S.U.; Dincer, I. A Study on Comparative Environmental Impact Assessment of Thermochemical Cycles and Steam Methane Reforming Processes for Hydrogen Production Processes. *Comput. Chem. Eng.* **2024**, *180*, 108514. [CrossRef]
17. Aydin, M.I.; Dincer, I. Comparative Modeling and Assessment of Renewable Hydrogen Production and Utilization in Remote Communities. *Comput. Chem. Eng.* **2025**, *194*, 108995. [CrossRef]
18. Karczewski, M.; Chojnowski, J.; Szamrej, G. A Review of Low-CO2 Emission Fuels for a Dual-Fuel RCCI Engine. *Energies* **2021**, *14*, 5067. [CrossRef]
19. Szamrej, G.; Karczewski, M. Exploring Hydrogen-Enriched Fuels and the Promise of HCNG in Industrial Dual-Fuel Engines. *Energies* **2024**, *17*, 1525. [CrossRef]
20. Falfari, S.; Cazzoli, G.; Mariani, V.; Bianchi, G.M. Hydrogen Application as a Fuel in Internal Combustion Engines. *Energies* **2023**, *16*, 2545. [CrossRef]
21. Beccari, S.; Pipitone, E.; Caltabellotta, S. Analysis of the Combustion Process in a Hydrogen-Fueled CFR Engine. *Energies* **2023**, *16*, 2351. [CrossRef]

22. Kumaraswamy, A.; Garud, S.S.; Karimi, I.A.; Farooq, S. Hydrogen for Net-Zero Emissions in ASEAN by 2050. *Int. J. Hydrogen Energy* **2024**, *90*, 575–587. [CrossRef]
23. Aghahasani, M.; Gharehghani, A.; Mahmoudzadeh Andwari, A.; Mikulski, M.; Pesyridis, A.; Megaritis, T.; Könnö, J. Numerical Study on Hydrogen–Gasoline Dual-Fuel Spark Ignition Engine. *Processes* **2022**, *10*, 2249. [CrossRef]
24. Nunes, F.C.; Vara Prasad, M.N.; Alves, L.D.J. Contribution of Hydrogen Economy toward Net Zero Emission and Decarbonization. In *Accelerating the Transition to a Hydrogen Economy*; Elsevier: Amsterdam, The Netherlands, 2025; pp. 59–76, ISBN 978-0-443-14039-6.
25. Molina, S.; Ruiz, S.; Gomez-Soriano, J.; Olcina-Girona, M. Impact of Hydrogen Substitution for Stable Lean Operation on Spark Ignition Engines Fueled by Compressed Natural Gas. *Results Eng.* **2023**, *17*, 100799. [CrossRef]
26. Sterlepper, S.; Fischer, M.; Claßen, J.; Huth, V.; Pischinger, S. Concepts for Hydrogen Internal Combustion Engines and Their Implications on the Exhaust Gas Aftertreatment System. *Energies* **2021**, *14*, 8166. [CrossRef]
27. Le, D.K.; Kwon, H.; Lee, M.J. Numerical and Experimental Investigation of the Correlation between Inlet Flow Rates, Temperature, and NOx Emissions in Pure Hydrogen Combustion. *Appl. Therm. Eng.* **2025**, *259*, 124748. [CrossRef]
28. Caricato, A.; Carlucci, A.P.; Potenza, M.E.C.; Laforgia, D.; Torresi, M.; Strafella, L. Autoignition Characterization of Hydrogen Directly Injected into a Constant-Volume Combustion Chamber through a Heavy-Duty Injector. *Energies* **2023**, *16*, 6823. [CrossRef]
29. Giacomazzi, E.; Troiani, G.; Di Nardo, A.; Calchetti, G.; Cecere, D.; Messina, G.; Carpenella, S. Hydrogen Combustion: Features and Barriers to Its Exploitation in the Energy Transition. *Energies* **2023**, *16*, 7174. [CrossRef]
30. Al-Janabi, H.A.-K.S.; Al-Baghdadi, M.A.-R.S. A Prediction Study of the Effect of Hydrogen Blending on the Performance and Pollutants Emission of a Four Stroke Spark Ignition Engine. *Int. J. Hydrogen Energy* **1999**, *24*, 363–375. [CrossRef]
31. Akif Ceviz, M.; Sen, A.K.; Küleri, A.K.; Volkan Öner, İ. Engine Performance, Exhaust Emissions, and Cyclic Variations in a Lean-Burn SI Engine Fueled by Gasoline–Hydrogen Blends. *Appl. Therm. Eng.* **2012**, *36*, 314–324. [CrossRef]
32. Ji, C.; Cong, X.; Wang, S.; Shi, L.; Su, T.; Wang, D. Performance of a Hydrogen-Blended Gasoline Direct Injection Engine under Various Second Gasoline Direct Injection Timings. *Energy Convers. Manag.* **2018**, *171*, 1704–1711. [CrossRef]
33. Meng, H.; Ji, C.; Yang, J.; Wang, S.; Chang, K.; Xin, G. Experimental Study of the Effects of Excess Air Ratio on Combustion and Emission Characteristics of the Hydrogen-Fueled Rotary Engine. *Int. J. Hydrogen Energy* **2021**, *46*, 32261–32272. [CrossRef]
34. Qiang, Y.; Zhao, S.; Yang, J.; Cai, J.; Su, F.; Wang, S.; Ji, C. Effect of Excess Air Ratio and Spark Timing on the Combustion and Emission Characteristics of Turbulent Jet Ignition Direct Injection Hydrogen Engine. *Int. J. Hydrogen Energy* **2024**, *93*, 1166–1178. [CrossRef]
35. Lee, J.; Park, C.; Bae, J.; Kim, Y.; Choi, Y.; Lim, B. Effect of Different Excess Air Ratio Values and Spark Advance Timing on Combustion and Emission Characteristics of Hydrogen-Fueled Spark Ignition Engine. *Int. J. Hydrogen Energy* **2019**, *44*, 25021–25030. [CrossRef]
36. Liang, Z.; Xie, F.; Jiang, B.; Li, X.; Su, Y.; Wang, Z. Evaluating the Potential of Mixture Formation Methods to Achieve Efficient Combustion and Near-Zero Emissions on a Hydrogen Direct Injection Engine. *J. Clean. Prod.* **2024**, *439*, 140930. [CrossRef]
37. Di Profio, P.; Canale, V.; Germani, R.; Arca, S.; Fontana, A. Reverse Micelles Enhance the Formation of Clathrate Hydrates of Hydrogen. *J. Colloid Interface Sci.* **2018**, *516*, 224–231. [CrossRef] [PubMed]
38. Durkin, K.; Khanafer, A.; Liseau, P.; Stjernström-Eriksson, A.; Svahn, A.; Tobiasson, L.; Andrade, T.S.; Ehnberg, J. Hydrogen-Powered Vehicles: Comparing the Powertrain Efficiency and Sustainability of Fuel Cell versus Internal Combustion Engine Cars. *Energies* **2024**, *17*, 1085. [CrossRef]
39. Gültekin, N.; Ciniviz, M. Experimental Investigation of the Effect of Hydrogen Ratio on Engine Performance and Emissions in a Compression Ignition Single Cylinder Engine with Electronically Controlled Hydrogen-Diesel Dual Fuel System. *Int. J. Hydrogen Energy* **2023**, *48*, 25984–25999. [CrossRef]
40. Lin, Y.-C.; Lin, S.-L.; Jhang, S.-R.; Chen, K.-S.; Su, C.-W.; Huang, C.-E. Energy Saving and Pollutant Emission Reduction by Adding Hydrogen in a Gasoline-Fueled Engine. *Aerosol Air Qual. Res.* **2022**, *22*, 220259. [CrossRef]
41. Gabana, P.; Giménez, B.; Martín Herreros, J.; Tsolakis, A. Analysis of the Combustion Speed in a Spark Ignition Engine Fuelled with Hydrogen and Gasoline Blends at Different Air Fuel Ratios. *Fuel* **2025**, *381*, 133563. [CrossRef]
42. Padmanabhan, S.; Punitha, N.; Poyyamozhi, N.; Senthil, S.; Damodharan, D.; Sakunthala, K. Sustainability Improvement of Spark-Ignition Engine Performance Enhanced with Nanoparticles and Hydroxy Gas. *Int. J. Hydrogen Energy* **2024**, *96*, 1171–1185. [CrossRef]
43. Zhang, R.; Shu, G.; Zhao, H.; Chen, L.; Wei, H.; Pan, J. A Comparative Study on NH3/H2 and NH3/CH3OH Combustion and Emission in an Optical SI Engine. *Fuel* **2024**, *369*, 131731. [CrossRef]
44. Fontaras, G.; Ciuffo, B.; Zacharof, N.; Tsiakmakis, S.; Marotta, A.; Pavlovic, J.; Anagnostopoulos, K. The Difference between Reported and Real-World CO_2 Emissions: How Much Improvement Can Be Expected by WLTP Introduction? *Transp. Res. Procedia* **2017**, *25*, 3933–3943. [CrossRef]
45. Anticaglia, A.; Balduzzi, F.; Ferrara, G.; De Luca, M.; Carpentiero, D.; Fabbri, A.; Fazzini, L. Feasibility Analysis of a Direct Injection H2 Internal Combustion Engine: Numerical Assessment and Proof-of-Concept. *Int. J. Hydrogen Energy* **2023**, *48*, 32553–32571. [CrossRef]

46. Li, Y.; Gong, J.; Deng, Y.; Yuan, W.; Fu, J.; Zhang, B. Experimental Comparative Study on Combustion, Performance and Emissions Characteristics of Methanol, Ethanol and Butanol in a Spark Ignition Engine. *Appl. Therm. Eng.* **2017**, *115*, 53–63. [CrossRef]
47. Liu, X.; Wang, H.; Zheng, Z.; Liu, J.; Reitz, R.D.; Yao, M. Development of a Combined Reduced Primary Reference Fuel-Alcohols (Methanol/Ethanol/Propanols/Butanols/n-Pentanol) Mechanism for Engine Applications. *Energy* **2016**, *114*, 542–558. [CrossRef]
48. Rimkus, A.; Matijošius, J.; Bogdevičius, M.; Bereczky, Á.; Török, Á. An Investigation of the Efficiency of Using O_2 and H_2 (Hydrooxile Gas -HHO) Gas Additives in a Ci Engine Operating on Diesel Fuel and Biodiesel. *Energy* **2018**, *152*, 640–651. [CrossRef]
49. Rimkus, A.; Mejeras, G.; Dittrich, A.; Pukalskas, S.; Barta, D. Effect of the Concentration of Bioethanol Mixed with Gasoline on the Energy and Environmental Performance of a Hybrid Vehicle in the Worldwide Harmonized Light Vehicles Test Cycle (WLTC). *Appl. Sci.* **2024**, *14*, 10858. [CrossRef]
50. Duan, X.; Feng, L.; Chu, X.; Sun, Z. The Performance of a Spark Ignition Gasoline Engine with Hydrogen Addition under Low-Load Conditions. *Fuel* **2025**, *379*, 133091. [CrossRef]
51. Purayil, S.T.P.; Hamdan, M.O.; Al-Omari, S.; Selim, M.; Elnajjar, E. Influence of Ethanol–Gasoline–Hydrogen and Methanol–Gasoline–Hydrogen Blends on the Performance and Hydrogen Knock Limit of a Lean-Burn Spark Ignition Engine. *Fuel* **2024**, *377*, 132825. [CrossRef]
52. Manzoor, M.U.; Dou, X.; Yosri, M.; Talei, M.; Yang, Y. Capturing Different Modes of Hydrogen Combustion in a Spark-Ignition Engine Using Numerical Simulations. *Fuel* **2024**, *375*, 132343. [CrossRef]
53. Duan, X.; Chu, X.; Wang, R.; Chen, Z.; Zhou, F.; Abdellatief, T.M.M. The Performance and Emissions Characteristics of the Gasoline Spark Ignition Engine Fuelled with Green and Renewable Methanol and Hydrogen. *Renew. Energy* **2025**, *240*, 122184. [CrossRef]
54. Purayil, S.T.P.; Hamdan, M.O.; Al-Omari, S.A.B.; Selim, M.Y.E.; Elnajjar, E. Impact of Intake Air Pressure and Temperature on Performance and Hydrogen Knock Limit in a Spark-Ignition Engine Using Hydrogen-Gasoline Blends. *Appl. Therm. Eng.* **2025**, *263*, 125331. [CrossRef]
55. Marchitto, L.; Costagliola, M.A.; Berra, A. Influence of Performance Packages on Fuel Consumption and Exhaust Emissions of Passenger Cars and Commercial Vehicles under WLTP. *Energies* **2024**, *17*, 3356. [CrossRef]
56. Purayil, S.T.P.; Martini, E.A.; Elsaid, A.; Khalil, M.; Zoghbour, T.; Seyam, M.; Elnajjar, E. Influence of Steam Induction on the Performance and Hydrogen Knock Limit of a Hydrogen-Gasoline Spark Ignition Engine. *Int. J. Thermofluids* **2024**, *24*, 100933. [CrossRef]
57. Karagöz, Y. Analysis of the Impact of Gasoline, Biogas and Biogas + Hydrogen Fuels on Emissions and Vehicle Performance in the WLTC and NEDC. *Int. J. Hydrogen Energy* **2019**, *44*, 31621–31632. [CrossRef]
58. Barbu, M.C.; Birtaş, A.; Chiriac, R. On the Improvement of Performance and Pollutant Emissions of a Spark Ignition Engine Fuelled by Compressed Natural Gas and Hydrogen. *Energy Rep.* **2022**, *8*, 978–991. [CrossRef]
59. DIESELNET Emission Standards: Europe: Cars GHG. Available online: https://dieselnet.com/standards/eu/ghg.php (accessed on 17 December 2024).
60. European Parliament and of the Council. *Regulation (EU) 2019/631*; European Parliament and of the Council: Brussels, Belgium, 2019; Volume 111.

Disclaimer/Publisher's Note: The statements, opinions and data contained in all publications are solely those of the individual author(s) and contributor(s) and not of MDPI and/or the editor(s). MDPI and/or the editor(s) disclaim responsibility for any injury to people or property resulting from any ideas, methods, instructions or products referred to in the content.